



Coupled fluid-structure-interaction simulation approach for correction of the thermal tool elongation to improve the milling precision

Steffen Brier¹ · Lukáš Topinka¹ · Joachim Regel¹ · Martin Dix^{1,2}

Received: 24 January 2024 / Accepted: 7 June 2024
© The Author(s) 2024

Abstract

During milling operation, the position of the tool centre point (TCP) is affected by structural displacements, which are caused by force loads and heat input inside the machine as well as machining induced thermal loads. These thermal loads result in considerable thermal deformations of tool holder, tool, and accordingly the TCP position. They can be summed up to about tens of microns and compromise the dimensional accuracy. The objective was to develop an integrated, numerical simulation-based approach for future TCP correction for a milling process using characteristic diagrams. For this, a complex Fluid-Structure-Interaction (FSI) simulation model predicts the uni-axial displacement in the longitudinal direction of the TCP due to a specified process heat source at the tool tip. As a partial result, the simulation has reached its performance limits, under the restriction of a reasonable simulation time in order to produce characteristic diagrams for application on a milling machine. The calculated thermally induced displacement can be further processed with the aid of Design of Experiments (DoE) and response surface methodology (RSM), depending on the thermal process load and coolant volume flow rate. That results in characteristic diagrams for the displacement as a function of process parameters. In this study the calculated value for thermally induced TCP displacement covers a span from 10 μm to 80 μm , with a strongly nonlinear behaviour. Subsequently, this forms the basis for a future implementation of characteristic diagrams in the machine control system for online correction of thermal tool errors.

✉ Steffen Brier
steffen.brier@mb.tu-chemnitz.de

Lukáš Topinka
lukas.topinka@mb.tu-chemnitz.de

Joachim Regel
joachim.regel@mb.tu-chemnitz.de

Martin Dix
martin.dix@mb.tu-chemnitz.de

¹ Institute for Machine Tools and Production Processes,
Chemnitz University of Technology, Reichenhainer
Straße 70, 09126 Chemnitz, Germany

² Fraunhofer Institute for Machine Tools and Forming
Technology IWU, Reichenhainer Straße 88, 09126 Chemnitz,
Germany

Gekoppelte Simulation der Fluid-Struktur-Wechselwirkung für die Korrektur der thermischen Werkzeugdehnung zur Verbesserung der Präzision in der Fräsbearbeitung

Zusammenfassung

Im Verlauf der spanenden Fräsbearbeitung wird die Position des Tool Centre Points (TCP) durch strukturelle Verformungen beeinflusst, welche zum einen durch die Prozesskräfte zum anderen aufgrund der prozessinduzierten Wärmelasten verursacht werden. Diese Verformungen können im Bereich von Zehntelmillimetern liegen und die Fertigungsgenauigkeit negativ beeinflussen. Ziel dieser Arbeit war die Entwicklung einer ganzheitlichen numerisch basierten Methode, die mittels charakteristischer Diagramme die prozessinduzierten TCP Verlagerungen korrigiert. Für diesen Zweck wurde ein komplexes Fluid-Structure-Interaction (FSI) Simulationsmodell konzipiert, das die einachsigen TCP Verschiebungen in Werkzeuglängsrichtung berechnet, welche aus einer spezifischen Prozesswärmequelle an der Werkzeugspitze resultieren. Hierbei reizte das Simulationsmodell die Leistungsgrenze aus, unter der Randbedingung einer vertretbaren Simulationsdauer, um die charakteristischen Diagramme für die betrachtete Fräsmaschine zu erzeugen. Die berechneten thermisch induzierten TCP Verschiebungen können mittels Einsatz der statistischen Versuchsplanung (DoE) und der Response Surface Methode (RSM) weiterverarbeitet werden, um die Abhängigkeit von der thermischen Prozesslast und dem Kühlmittelvolumenstrom darzustellen. Daraus resultieren charakteristische Diagramme für die Verschiebung als Funktion der Prozessparameter. In dieser Untersuchung reichte die Spanne der thermisch induzierten TCP Verschiebung von $10\ \mu\text{m}$ bis $80\ \mu\text{m}$ und wies dabei ein hochgradig nichtlineares Verhalten auf. Diese Erkenntnisse bilden die Grundlage für eine zukünftige Einbindung der charakteristischen Diagramme in die Maschinensteuerung, für die online Korrektur des thermischen Fehlers.

1 Introduction

The increasing demands on quality and dimensional accuracy of machining require a profound understanding of the machining process. This includes the mechanical process of chip removal as well as an extensive understanding of the thermal processes in the cutting zone, which addresses an essential role in machining accuracy. In a milling process, involving the use of cooling lubricants, multiple heat sources and sinks must be considered. A significant amount of heat is produced in the chip formation process, besides the forming due to plastic material deformation, by friction at the contact of the cutting tool, chip and workpiece. These thermal loads cause thermo-elastic deformations of the tool. Such result in a displacement of the tool centre point (TCP) which influences the machining precision [1].

Furthermore, while milling an additional heat flow from the spindle contributes to the thermal load of the tool holder and the tool. It is introduced by heat transfer at the tool interface into the tool holder and contributes to the TCP displacement [2].

These multiple thermal loads cause thermo-elastic deformations of the tool and the workpiece. The present tendency to achieve accurate and precise machining is contrary to recently described thermo-elastic deformations in the milling processes. In some machining cases 75% of geometric errors of the workpiece are caused by thermal influences [3]. The results of a recent survey state that on average, 62% of the total error is thermally induced according to estimations of machine tool manufacturers [4].

2 State of the art

In the context of the challenges of modern production in the border areas of manufacturing, also correction of TCP displacement is necessary to meet the ever-increasing quality requirements. In this context, it is necessary to dovetail simulation and production to achieve the set goals.

The quantification of a cutting process heat load depends on a wide range of influences. Several researchers developed different approaches to predict the ratio of heat, which is dissipated into tool, chips and workpiece [5–9]. The statements regarding the size of partition are widely divergent and the precise share is dependent on the applied cutting parameters. The relevant heat partition, which is causing the heat flow into the tool, varies between 1 to 20% [5]. With increasing cutting speed the partition of heat into the chips rises and the heat dissipation into the tool and the workpiece is decreasing [10–12]. Another thermal load on the tool is induced in form of heat flow from the spindle interface and contributes to the temperature increase of the tool-tool holder system [13].

Several researchers considered the thermal structural deformation of the entire machine tool, excluding the process induced heat flow into the tool and the tool holder and the resulting interaction with cooling media and their impact on the TCP displacement [14–16]. The influence of a single-phase air flow on the thermo-elastic behaviour of the tool and tool holder was thoroughly investigated in [17] and [18]. They developed a simulation model to describe the temperature behaviour of the tool-tool holder system under the influence of a cooling air jet fed by a nozzle. The investigation showed that the temperature of the coolant has only

Table 1 Regression analysis

Nomenclature and Acronyms		
α	in $1/^\circ\text{C}$	Thermal expansion coefficient
β	in ...	Regression coefficient
γ	in $^\circ$	Angle
$\widehat{\varepsilon}_{\text{th}}$	in –	Strain tensor
E	in MPa	Young modulus
η	in Pa s	Dynamic viscosity
θ	in $^\circ\text{C}$	Temperature
$\Delta\theta$	in $^\circ\text{C}$	Temperature difference
$\Delta\theta_{\text{error}}$	in $^\circ\text{C}$	Absolute temperature error
θ_i	in $^\circ\text{C}$	Local temperature
θ_{ref}	in $^\circ\text{C}$	Reference temperature
θ_{sim}	in $^\circ\text{C}$	Simulated temperature
θ_{qss}	in $^\circ\text{C}$	Steady-state temperature
$\theta_{\bar{x}}$	in $^\circ\text{C}$	Mean steady-state temp.
λ	in W/mK	Heat conductivity
ν	in –	Poisson ratio
τ	in s	Time constant
ρ	in kg/m^3	Density
CI	in $^\circ\text{C}$	Confidence interval
CSF	in N	Continuum Surface Force
c_p	in W/kgK	Specific heat capacity
DoE	in –	Design of experiments
FSI	in –	Fluid-Structure-Interaction
F_c	in N	Cutting force
n	in –	Sample size
P_c	in W	Cutting power
P_{ind}	in W	Inductive power
\dot{Q}_{cut}	in W	Heat proportion of the tool
s_x	in $^\circ\text{C}$	Standard deviation
SER	in μm^2	Standard error of regression
SSE	in μm^2	Sum of squares explained
t	in s	Time
t_v	in –	Value of t distribution
$T1 - T4$	in –	Temperature sensors
TCP	in –	Tool center point
ΔTCP	in μm	TCP displacement
$\widehat{\Delta TCP}$	in μm	Predicted TCP displacement
R	in –	Correlation coefficient
RMSE	in μm	Root mean squared error
v_c	in m/min	Cutting speed
\dot{V}_{cool}	in l/min	Coolant flow rate
x	in mm	Distance in x
\bar{x}	in $^\circ\text{C}$	Mean temperature
y	in mm	Distance in y

a small impact on the temperature distribution compared to the air velocity. Subsequently, the simulation models were further developed to take a liquid cooling phase and tool rotation into account regarding the calculation of the tool and tool holder temperature field [19]. The simulation showed

a reduced heat exchange of the tool with the coolant fluid if the tool was rotating. To narrow the gap between simulation and reality, a multiphase CFD simulation model was developed, which allows the simulation of dispersed coolant flow around the rotating tool and holder surface [20]. Optical comparisons of the flow field led to a good agreement with the flow field at the testing rig. Following this, the Computational Fluid Dynamics CFD simulation was coupled with a structural-mechanical model in order to calculate the resulting TCP displacement of tool and tool holder due to the thermal boundary conditions [21]. In recent times, the machining investigations using FSI concentrated especially on chip formation and the thermo-mechanical conditions under the influence of cutting fluid. These models include mostly chip formation and are situated in micro- or mesoscale [22].

Other researchers developed macro scale models of the whole tool to analyse the coolant impact on the structure. Some aimed to utilize CFD to investigate the liquid Nitrogen delivery system of an internal cooled end mill and analysed the interaction between coolant and cutting zone [23]. A significant impact of nozzle geometry, process conditions, cavitation formation, coolant pressure, and transport efficiency was highlighted. The simulation model neglected the tool rotation. Others used an ANSYS Fluent model to design a pressurized internal cooling milling cutter for milling nickel based alloys [24]. Both studies can hardly be transferred to external cooling, due to the focus on the method of internal cooling and in case of the coolant fluid [23]. The resulting TCP displacement was also neglected.

Some investigations aimed to correct the thermal error, the calculated values of the machine tool deformation form the basis for correction via several methods to increase the machining accuracy [25–27]. In particular, characteristic diagram method was intensively researched due to its suitability for integration into the machine control system and thus online correctability. The characteristic diagram can be utilized to decouple fluid and thermo elastic simulations in the context of heat transfer coefficient calculation [25]. The approximation of an characteristic TCP diagram based on measured temperatures at two different points was investigated in [26]. This TCP displacement approximations have been very accurate but they only considered a single, fixed kinematic configuration of the machine tool. The dependency of artificial intelligence based approaches on the achievable prediction quality is influenced by the selected input parameters for the characteristic diagram and the training data was analysed in [27]. A new method developed for updating characteristic diagram based correction models by combining existing models with new measurements was presented in [28]. This allows the optimization of the correction for serial production load cases without the effort of computing a new model.

Due to the causal relationship between the considered input variables and the resulting TCP displacement, the method of characteristic diagrams is particularly well suited due to the clear mathematical structure of the regression equation, which enables processing by the machine control system in real time with low latencies. For correction of the tool elongation under cutting fluid influence a considerably different model is needed, which translocates the FSI in a macro-scale environment, calculates the temperature of the aggregated tool-tool holder structure and enables a combination of the characteristic diagram method based on thermally induced simulated TCP displacements with the coupled FSI model.

Based on the state of the art, it can be concluded that the interaction between the rotating milling tool and the cutting fluid is a little noticed area of research by numerical methods in the field of thermally induced TCP displacement. It is hypothesised that the behaviour of the thermally induced TCP displacement is highly non-linear due to the interactions with the coolant and can be described by means of a regression function. This leads to the necessity for a more intensive analysis using simulative coupled CFD and FEM tools. An understanding of the thermal TCP displacement would provide a partial contribution to the future development of an online correction method, which would lead to an improvement in the accuracy of milling operations.

3 Aims and approach

The aim of this work is to derive a characteristic diagram dependent on the process parameters, such as coolant flow rate, the cutting process heat load and the rotational speed, which represents the displacement behaviour of the tool and the tool holder to calculate the TCP displacement of the tool–tool holder system. To achieve this goal, several methods were utilised.

Initially, an unidirectional transient fluid-structure interaction FSI macro model of the tool Fig. 1 and the tool holder for the application of cooling lubricant in the form of full jet cooling was developed [21]. The reason for the application of the FSI is the possibility to cover the thermo-elastic behaviour of the TCP under full jet cooling, which requires a coupled simulation approach of CFD and structural calculations. It combines a two-phase turbulence fluid flow model of cooling lubricant around a rotating cutting tool with the structural thermo-elastic simulation. The result of this coupling will be a simulation of the TCP displacement depending on the abstracted process-induced machining heat, rotational speed of the cooled cutting tool surface and the applied volume of cooling lubricant flow. The calculated temperature field of the tool and tool holder will

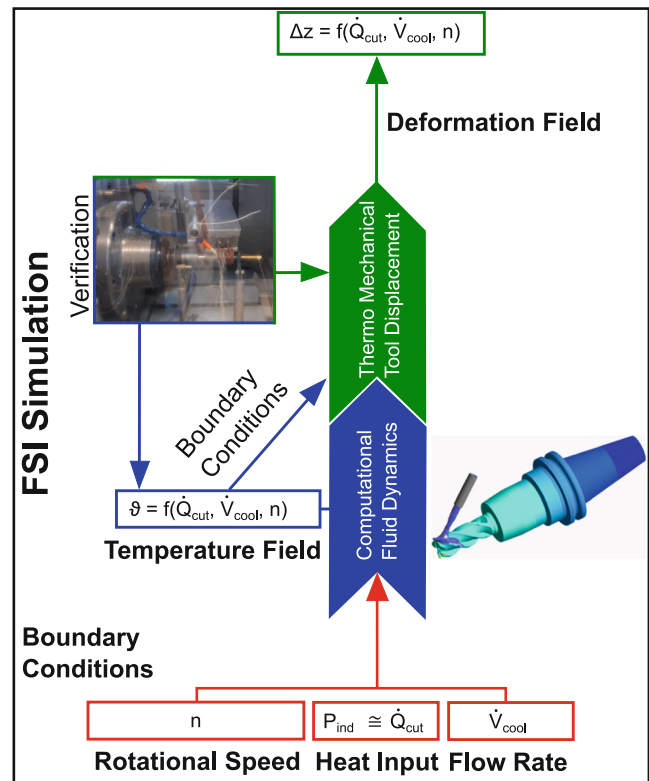


Fig. 1 FSI scheme of the coupled simulation approach

be finally compared with experimental data to verify the model quality.

In order to achieve the goal of characteristic diagram a statistical test plan and multi-variant regression will be utilized. The DoE delivers the methodology to construct test plan designs to gather data with a manageable amount of runs and resource deployment. The developed FSI model was applied to calculate the axial TCP displacement according to the chosen experimental design, a full-factorial design with 12 simulation runs. Finally, the multi-variant regression will be used to process the calculated TCP displacements. With the aid of a non-linear quadratic regression model a characteristic diagram will be generated. This characteristic diagram will show the correlation of the heat load of the tool and applied coolant.

4 Model for thermal FSI coupling

The first step is the definition of the heat source, which represents the cutting process. Subsequently, the thermal-fluid model of the FSI is calculating the body temperature field due to conjugated heat transfer for the observed parameter set. Basis of the CFD is the applied homogeneous Euler-Euler approach and the assumption that the different phases are homogeneous. This kind of multiphase flow

refers to the case where shared velocity fields and other relevant fields exist for each fluid, they share also a pressure field and the fluids are not interacting via inter-phase transfer terms. The terminology “conjugated heat transfer” describes a heat transfer process between a solid body and a flowing fluid through forced convection [29]. Afterwards, the calculated temperature field of the tool and tool holder is transferred via unidirectional coupling between fluid analysis and structural analysis as a thermal boundary condition. A unidirectional thermal FSI is chosen, to transfer the body temperature field of tool and tool holder to a structural FEM model. The resulting displacement of the structure due to impact of the coolant jet could be also transferred, because of the low velocity ($< 2 \text{ m/s}$) no significant deformation of the tool is expected and therefore only temperature data is transferred. A continuous entering, leaving as well as re-cooling of the coolant takes place. Therefore, a reverse temperature data transfer was neglected. Because of the existent temperature gradients in the solid domain, the body is expanding and therefore the TCP is changing its spatial location. The subsequent calculation of the resulting TCP displacement and thermal characteristics are completing the introduced FSI methodology. The complete computational fluid dynamics and thermal-structural boundary conditions are illustrated in Fig. 1.

5 Experimental verification of the CFD model

During machining, the heat load into the tool is largely concentrated in a small area. Additionally, the amount of heat, which is introduced in the tool, depends on the process parameters. Without a sufficient definition of the heat source, a verification of the FSI model is not possible due to the lack of reasonable boundary conditions. The heat source of the milling process was simplified and replaced by an inductive heat source P_{ind} , which is only present on the end mill surface and a thin layer below. At the tool axis, the value of the heat is approximately zero. Induction heating is physically based on Faraday’s law of induction. An electromagnetic field simulation with ANSYS Maxwell was conducted to quantify the volumetric heat loss distribution induced in the end mill [30]. Subsequently, the verification of the body temperature calculation via CFD simulation in the developed FSI model for the TCP displacement was conducted.

The metrological investigations were carried out on a testing stand, which is predestined for thermal analyses in particular [31]. It consists of a machine bed on which a horizontally aligned motor spindle of type 2SP1253 from the manufacturer Weiss is mounted (Fig. 2). An enclosure shields the working space from the environment. The

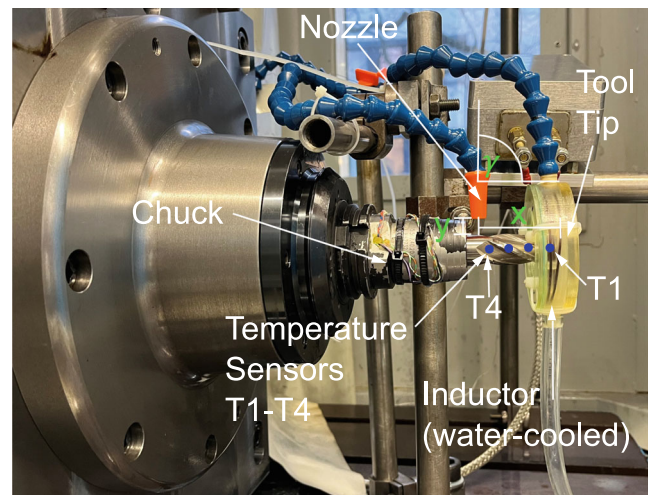


Fig. 2 Testing stand for induction heating

tool, made of HSS-E, and the tool holder, made of hot work steel, can be heated in the same way as in the real machining process by a specially designed induction system. Pt100 sensors were implemented along the axis of the 20 mm diameter end mill tool to measure the temperature at defined positions till the steady-state was reached. The four Pt100 sensors are positioned at 10 mm (T1), 20 mm (T2), 35 mm (T3) and 55 mm (T4) distance to the tool tip on the rotation axis of the hollow drilled end mill. The sensor data is passed through the drill hole of the tool via wiring and then the measuring signals are transmitted due to a slip ring at the rear end of the spindle. From there, the measurement signals are amplified and transferred to a PC for subsequent storing and visualisation (Matlab/LabVIEW).

The nozzle introduces the coolant in carefully dosed amounts, which is a water-oil emulsion named Aerolan 2200 [32]. Relevant dimensions are the tool diameter 20 mm and nozzle related dimensions, like nozzle diameter 6 mm, horizontal distance to tool tip $x = 50 \text{ mm}$, vertical distance to the end mill surface $y = 10 \text{ mm}$, and the nozzle alignment to the rotational axis of the tool is $\gamma = 90^\circ$. All necessary experimental measurements for the heated end mill under coolant flow were replicated three times to gather certainties of scattering of the measured temperature values. Due to the sample size of measured steady-state temperature data and in accordance to the central limit theorem in the probability theory the t -distribution was used to calculate the confidence intervals for the temperature curve data for each temperature sensor [33]. For the comparison of simulation and experiment, the steady-state value of the transient temperature curves was evaluated. The experimental plan of the temperature measurements consists of one varied factor, the heating power with four levels. The coolant flow rate and the rotational speed were kept constant. The Eq. (1) calculates the confidence interval [34], of the thermal stead-

Table 2 Material properties of solid components

Properties	HSS-E [41]	Hot Work Steel [41]
ρ in kg/m^3	8150	7780
c_p in J/kgK	420	460
λ in W/mK	27.4	25
E in GPa	230	215
ν in –	0.28	0.3
α in 10^{-6}K^{-1}	11.4	10.9

state for every sensor position for a defined confidence level (98%) with the sample standard deviation s_x , the number of samples n and the t -score t_v for the chosen confidence level.

$$CI_{\pm} = \bar{x} \pm t_v \frac{s_x}{\sqrt{n}} \tag{1}$$

$CI+$ is referred to as the upper and $CI-$ is designated as the lower confidence interval. Based on typical values for machining standard materials like AISI 1045 [35], the range of values for the heat source to be applied in the FSI model was determined with Eq. (2) [36].

$$\dot{Q}_{\text{cut}} = P_c \cdot 0.1 = F_c v_c \cdot 0.1 \tag{2}$$

For the milling of AISI 1045, the common values for cutting speed and cutting force were obtained from [37]. According to the obtained values, a reasonable span of heat energy input was determined (25 W, 75 W and 100 W). For the runs, the rotational speed was set to 600rpm and for the coolant volume flow rate a value of 11/min was chosen. In accordance to the experimental setup the same parameters were applied in the FSI simulation to permit a direct comparison of experiment and simulation. The initial temperature of the fluid and solid domains is stated with 20°C, the taper shank temperature is about 23°C and the cooling lubricant had a temperature of 22°C which is delivered via nozzle with a volume flow of 11/min. The initial volume fraction of the coolant in the fluid domain was zero. All material parameters for the solids and the fluids are defined in Tables 2 and 3.

The FSI simulation domain consists of a multiphase region where two continuous fluids are coexisting as presented in Fig. 3, the environmental air and the cooling lubricant.

In the simulation model, the heat load \dot{Q}_{cut} is applied via volumetric heat source field at the tool tip (Fig. 4), and is a mandatory thermal boundary condition in ANSYS CFX to calculate the resulting body temperature field. Further details regarding the process of the calculation of the volumetric heat loss field can be found in [30]. The Euler–Euler approach was applied to model the two distinct

Table 3 Material properties of fluids

Properties	Air [42]	DAW AEROLAN 2200 [32]
ρ in kg/m^3	1.185	940
c_p in J/kgK	1004.4	4183
λ in W/mK	0.0261	0.6
η in Pas	0.000018	0.009
α in K^{-1}	0.000336	0.0007

fluids. This method assumes that the involved phases are inter-penetrating, which is efficient when modelling macro scale process [38]. This includes an homogeneous flow field with separate velocity and turbulence equations ($k-\omega$ SST). The coolant fluid is defined as the first phase and the surrounding air as the second. Both fluids are treated as free surface flow for tracking and locating the air-coolant interface. In a real multiphase the air-coolant flow would be immiscible and leads to a tensile force along the phase interface, which is called surface tension force [39]. In the presented CFD model this force is modelled using the Continuum Surface Force (CSF) method presented in [40]. The CSF method incorporates an additional body force into the momentum equation of the navier-stokes equations, applies only for the cells in the inter-phase region [40] with a constant surface tension coefficient of 0.072 N/m. In the model, tool holder, tool and the fluid domain surrounding the tool rotate at the same speed (600rpm), avoiding the resource-intensive use of adaptive meshing for the area around the rotating tool. The meshing of the rotating domain was carried out using the inflation layer technique and included 10 layers with a total thickness of 0.1 mm. All other domains were meshed with tetrahedral elements. The total number of nodes was 512680. To find a appropriate time step, the

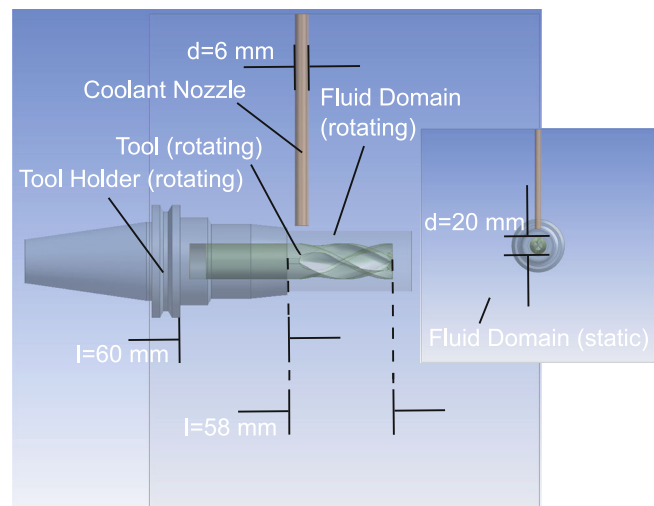


Fig. 3 FSI simulation domain in side and frontal view

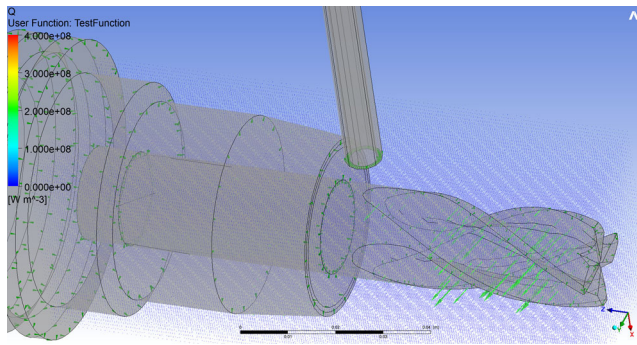


Fig. 4 Volumetric heat loss distribution as thermal BC

adaptive time-stepping method was utilized. More details of the CFD model set-up can be found in [21].

All thermal verification experiments were carried out using an extraction system, so the implementation of a corresponding boundary condition, in form of an outlet velocity (0.7 m/s measured) in the simulation model was considered, which represents the suction air flow in the simulation domain. The FSI model calculates the conjugated heat transfer between end mill, tool holder and surrounding

coolant. As an result, the steady-state temperature values at the sensor positions were benchmarked. In the graph (Fig. 5) the steady-state temperatures are displayed for the analysed heating power levels.

The low heating power of 25 W corresponds to finishing operation and 100 W to roughing operations. The diagram shows the temperature of the thermal steady-state of experiments and associated simulation for the four sensor positions. Due to the variety of the experimental data the upper and lower confidence interval for the thermal steady-state are also shown, besides the measured and simulated values. The Eq. (3) was utilized to calculate at each sensor position the absolute error $\Delta\theta_{error}$ of the simulated thermal steady-state θ_{sim} compared to the mean steady-state temperature $\theta_{\bar{x}}$ of all conducted experimental runs at each sensor position and specified in corresponding tables beside the graphs.

$$\Delta\theta_{error} = |\theta_{sim} - \theta_{\bar{x}}| \tag{3}$$

An analysis of the experimental temperature data shows an significant increase in scattering with higher heating power, which is noticeable in the widening of the confidence interval. The qualitative temperature progression of the experimental data is adequately covered by the simulation model. Except for the first sensor at the tool tip (T1), for 25 W power level, the simulation overestimated the tool temperature for every sensor. A comparison of the deviations between experiment and simulation shows that the difference is large even at an increased distance from the tool tip (T4), although the heat source is concentrated on the front part of the tool tip. The maximum difference $\Delta\theta_{error}$, which is in sensor position T2, ranges from 2.3 °C for 25 W to 6.6 °C for 75 W and 5.6 °C for 100 W heating power. These temperature discrepancies are clearly identifiable in the transient temperature graphs (Fig. 6), which are of particular interest in the heating of the rotating tool.

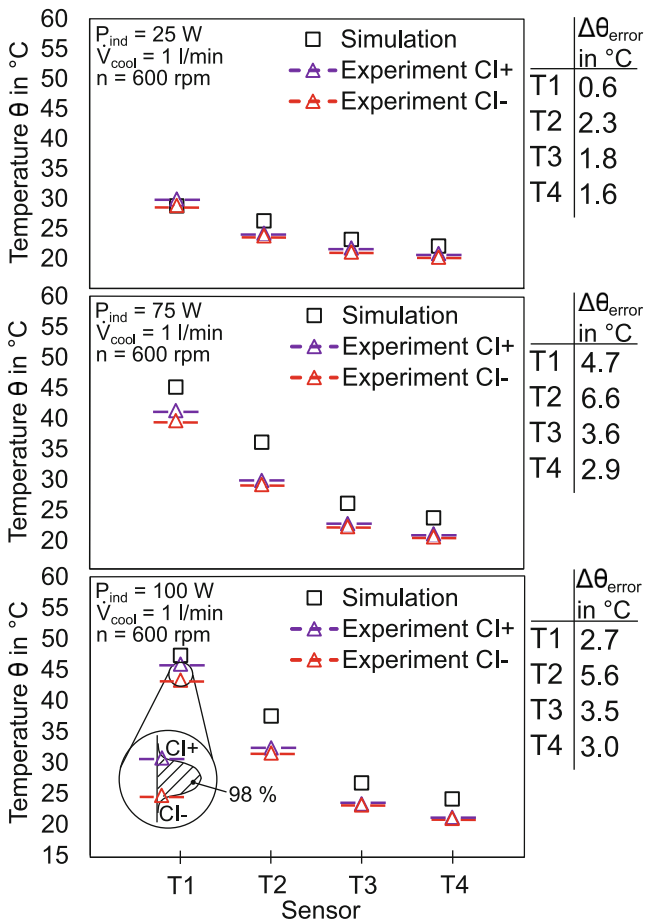


Fig. 5 Comparison of the thermal CFD simulation model

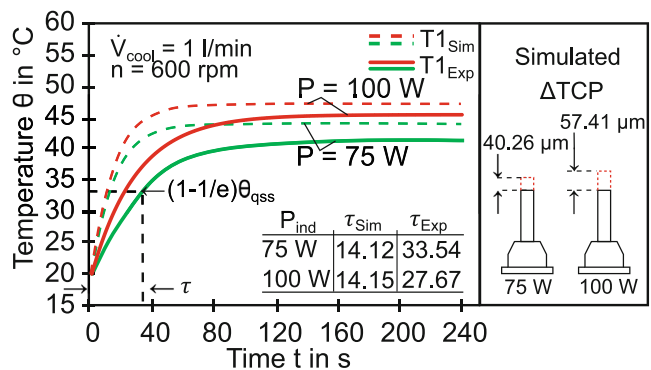


Fig. 6 Time behaviour of the tool tip temperature for T1

The transient behaviour is characterized by the thermal time constant τ in Eq. (4) [43].

$$\theta_i = \theta_{\text{ref}} + (\theta_{\text{qss}} - \theta_{\text{ref}})e^{-t/\tau} \quad (4)$$

This constant is defined as the time required for the material at a certain temperature to achieve 63.2% of the steady-state temperature. In this equation, the variable θ_{qss} is the steady-state temperature and θ_{ref} denotes the reference temperature. The time constant was calculated via least square regression of the transient temperature data for T1. A comparison of the time constants for the cases considered shows that the time constants of simulation and experiment differ. In case of the simulation (75 W and 100 W power level with $n = 600\text{rpm}$ and $\dot{V}_{\text{cool}} = 11/\text{min}$), the ratio of $\tau_{\text{exp}}/\tau_{\text{sim}}$ is about 2.37 and 1.96. For the sensor position T1, the time behaviour shows that especially for higher evaluated power levels the simulation reached a thermal steady-state within the first 120 seconds (Fig. 6). If the heat input is 100 W the difference between simulation and experiment is smaller than for 75 W. In case of 100 W heat load, the curves are approaching. The reason for the slightly higher time constant for 100 W heat input can be explained by the effect of the temperature ratio on the heat transfer coefficient. The higher surface temperature of the heated tool could lead to a minor increased heat transfer coefficient, because of the influence of the thermal boundary conditions (e.g., dynamic viscosity, density) on the grade of turbulence and therefore the heat transfer coefficient (reduced time constant) [44]. The deviations of the simulated time constants compared to the experimental can be explained by the inadequate transfer of the thermal energy from the tool to the coolant, because the heat dissipation from the tool into the coolant is undersized. As a result, the tool and tool holder reaches the thermal steady-state faster in the simulation compared to the experimental values. The resulting TCP displacement has been calculated with $40.25\ \mu\text{m}$ and $57.41\ \mu\text{m}$. The systematic overestimation of the temperature is based on a not correctly captured heat transfer between liquid and solid, due to a certain amount of heat energy remaining in the solid. The main challenge in the FSI simulation of the rotating end mill is the large scale of flow morphology and the necessity to resolve the fluid boundary layer. The quality of conjugate heat transfer is dependent on the mesh quality and element size of the boundary layer. Therefore, the overestimation of the measured temperature indicates that the heat transfer of the solids to the surrounding fluid is too low. At the area of the tool holder, the flow is nearly continuous and therefore description via free surface model is eligible, though in the area of the chip grooves, the coolant is dispersed into small droplets. The Algebraic Interface Area Density model AIAD could distinguish between the different flow field morphologies if the mesh elements are

too large [45]. A finer meshing of the boundary layer could also improve the model, as well as an enlargement of the simulation domain. This calms the flow before reaching the outlet of the domain and improves convergence. The consideration of the inductor geometry in the CFD simulation would improve the results. All approaches would increase the simulation time and some could complicate the convergence. Therefore an increase in computing performance would significantly improve the accuracy of the method presented. Referring to the assumption that the phase terms do not interact, it must be mentioned that in the case of temperatures at the tool surface equal or above the boiling point, the evaporation of the coolant phase must be taken into account. This would result in a non-negligible cooling effect due to the the vaporisation enthalpy. Neglecting the evaporation would lead to a massive overestimation of the tool temperature.

6 Characteristic diagram

The presented method refers to the thermal steady-state and the characteristic diagram is therefore only valid in this state. In order to generate a meaningful characteristic diagram, a representative parameter space has to be investigated. In the present work, two process parameters were varied, the inductor power level and the supplied coolant flow rate. A full factorial plan was chosen due to its high resolution regarding higher level interaction and non-linearity effects. For that the rotational speed parameter was assumed to be constant at 600rpm, process heat and coolant volume flow were varied. All simulated parameter combinations with four levels of process heat P_{ind} and three in coolant volume flow \dot{V}_{cool} as well as resulting simulated uni-axial displacements along the rotational tool axis are shown in Table 4.

Table 4 Experimental design and resulting calculated TCP displacement

P_{ind} in W	\dot{V}_{cool} in l/min	ΔTCP in μm
25	0	17.41
25	1	13.72
25	1.5	10.13
50	0	34.29
50	1	25.81
50	1.5	18.75
75	0	54.77
75	1	40.26
75	1.5	29.71
100	0	78.27
100	1	57.41
100	1.5	43.58

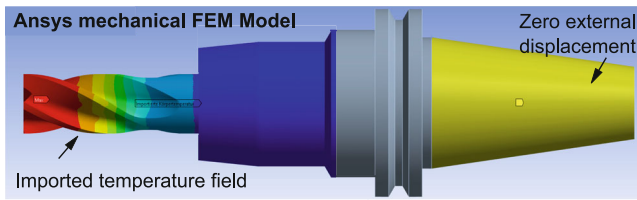


Fig. 7 Mechanical FEM model

The power was varied in steps of 25 W increments and the coolant flow rate was varied in three steps from 0l/min to 1l/min and 1.5l/min. The simulation model used complies exactly to the one presented in Sect. 4, all material data correspond to the values used in the verification simulations. All simulations were performed for a time span of 180s to ensure that the thermal steady-state condition occurs. After the resulting steady-state temperature fields for tool and tool holder have been calculated, a transfer to a structural mechanics model in the form of a thermal boundary condition takes place. The static ANSYS mechanical FEM model consists of the bodies of tool and tool holder and was meshed with 432094 tetrahedral structural elements of the type SOLID187, which are well suited to mesh complicated geometries. The shape of the tool and the tool holder made it impracticable to use other types of elements, such as structured hexahedral elements. The tetrahedral structural elements are a sufficient compromise between computational costs and model accuracy, without the disadvantages of overly model stiffness [46]. A zero external displacement in all spacial degrees of freedom was the only applied mechanical boundary condition to fix the taper shank of the tool holder (Fig. 7). The FEM model calculates the resulting TCP displacement with the aid of thermal strain induced by the temperature field (Eq. 5) and provides the base for construction of a regression model in form of a characteristic diagram [47].

$$\hat{\epsilon}_{th} = \alpha \Delta\theta = \alpha \Delta(\theta - \theta_{ref}) \tag{5}$$

Only the lengthwise displacement of the tool was evaluated, due to the necessity of absolute values for the TCP correction via offset value. The determined displacement values in longitudinal tool direction are subsequently used in a non-linear regression model to determine a mathemat-

Table 5 Coefficients of regression

Coefficients	
β_0 in μm	2.517
β_1 in $\mu\text{m}/\text{W}$	0.5305
β_2 in $\mu\text{m min}/\text{l}$	6.304
β_3 in $\mu\text{m min}/\text{Wl}$	0.002211
β_4 in $\mu\text{m min}^2/\text{l}^2$	-0.2341
β_5 in $\mu\text{m}/\text{W}^2$	-3.492

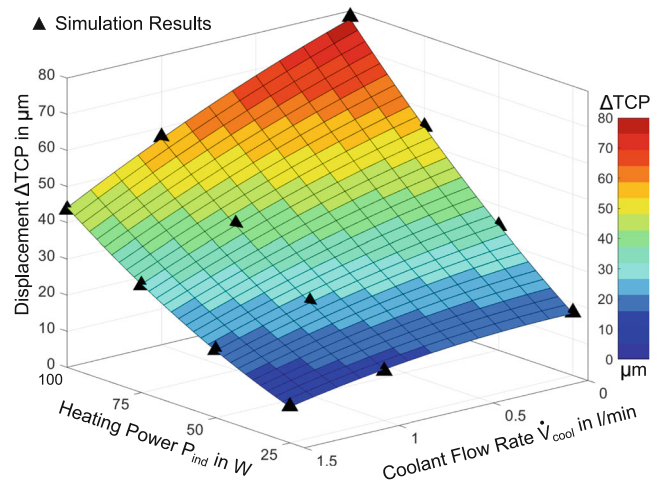


Fig. 8 Characteristic diagram for TCP displacement

ical function that describes the behaviour of the displacement in the longitudinal direction.

The regression model used is non-linear in order to map the expected curvature of the response surface, which describes the uni-axial displacement, in the parameter space [48]. By means of a non-linear quadratic regression equation (Eq. 6), the expected TCP displacement can be mathematically described as a function of the parameters heating power and coolant flow rate.

$$\begin{aligned} \Delta\widehat{TCP}(\dot{V}_{cool}, P_{ind}) = & \beta_0 + \beta_1 P_{ind} + \beta_2 \dot{V}_{cool} \\ & + \beta_3 \dot{V}_{cool} P_{ind} + \beta_4 \dot{V}_{cool}^2 + \beta_5 P_{ind}^2 \end{aligned} \tag{6}$$

The coefficients of the regression equation are listed in Table 5. A graphical representation of the calculated TCP displacement values over the parameter space shows the expected non-linear correlation between the process heat load, the coolant flow rate and the resulting uni-axial TCP displacement in all spacial directions of the investigated parameter space (Fig. 8).

The simulated displacement values range from 78.27 μm to 10.13 μm . For evaluation of the regression quality of linear models the R^2 value is very common in data analysis. In case of a non-linear regression, the R^2 shows a low performance to access the quality of the goodness of fit [49]. Although a R^2 of 0.9878 is significant high (Table 6), a more

Table 6 Regression analysis

Goodness of fit	
SSE in μm^2	1.3135
R^2 in -	0.9878
Adjusted R^2 in -	0.9558
SER in μm^2	0.2189
RMSE in μm	0.4678

appropriate statistical parameter for non-linear regression has been used. The standard error of the regression SER is the summed square of the deviation, by which the observed values differ from the regression surface [48]. For the applied model the SER is about $0.2189 \mu\text{m}^2$. More suitable to access the quality of a fit is the Root Mean Square Error RMSE, which is the standard deviation of the residuals. Residuals are a measure to quantify the distance to the regression surface data points. Therefore RMSE is a quantitative absolute value which is significantly small.

For the characteristic diagram of the TCP displacement, the regression surface values diverge on average from the simulated by $0.4678 \mu\text{m}$. This indicates a reasonable quality of the regression model. The non-linear multivariate quadratic model was identified as suitable for the construction of the characteristic diagrams. Based on the analysis of the regression model, it was concluded that the quality of the simulation model requires improvement to close the gap between simulation and experimental reality.

7 Summary, Conclusion and Outlook

The thermally induced dimensional and form deviations represent a major challenge for precision machining. For the series production of components with narrow dimensional and form tolerances, the thermally induced TCP displacement during production should be considered. In some cases, the dimensional tolerance is only a few μm large, and the TCP displacement can be several tens of μm . This leads to unintended machining errors. Numerical simulation models and characteristic diagram method can support to reduce the error. The coupled CFD-FEM simulation approach presented in this paper contains the calculation of the steady-state axial TCP displacement of a heated rotating end mill under the influence of coolant with the software ANSYS Workbench. This model calculates the resulting axial displacement values of the TCP at the thermal steady-state under different thermal process conditions like process heat and coolant flow rate. The progression of the tool temperature along the axis of rotation is qualitatively in good agreement reproduced by the simulation model. An overestimation of the tool temperature due to the model can be identified. Furthermore, the thermo-elastic behaviour of the longitudinal TCP displacement is highly non-linear and can be approximated with an quadratic regression model. The maximum displacement is about $78.27 \mu\text{m}$ (100 W, dry) and the minimum is $17,41 \mu\text{m}$ (25 W, 1.51/min). The developed method paves the way to derive characteristic diagrams as a function of process parameter values. High-quality response surfaces with minimal numerical effort could be derived with experimental plans based on Sobol sequence [50]. A derivation of transient correction values,

outside the thermal steady-state would require a large number of characteristic diagrams at different times up to the thermal steady-state to characterise the displacement behaviour in terms of time dependence. The necessary calculation time for the CFD simulations depends on the turbulence intensity of the flow field. The time required increases exponentially with increasing coolant flow rate and rotational tool speed.

A new method has been developed, which subsequently allows the integration of a characteristic diagram into the machine tool, in a similar way to Naumann et al. [28]. The next required step would be the verification of the simulated TCP displacement by means of experimental data and the subsequent integration of the resulting characteristic diagram in the machine tool to improve manufacturing precision.

Acknowledgements The authors would like to thank the German Research Foundation DFG for financial support within the CRC Transregio 96.

Funding The authors gratefully acknowledge financial support from the German Research Foundation DFG. The research was carried out within the framework of CRC Transregio 96 funded research. Project number: 174223256, Subproject A01 “Deformation of tool and clamping device” is part of the CRC.

Author Contribution All authors contributed to the study conception and design. Testing stand preparation, data collection and numerical analysis were performed by Steffen Brier and Lukáš Topinka. The manuscript was written by Steffen Brier. All authors commented on previous versions and approved the final manuscript.

Funding Open Access funding enabled and organized by Projekt DEAL.

Conflict of interest The authors declare no competing interests.

Open Access This article is licensed under a Creative Commons Attribution 4.0 International License, which permits use, sharing, adaptation, distribution and reproduction in any medium or format, as long as you give appropriate credit to the original author(s) and the source, provide a link to the Creative Commons licence, and indicate if changes were made. The images or other third party material in this article are included in the article’s Creative Commons licence, unless indicated otherwise in a credit line to the material. If material is not included in the article’s Creative Commons licence and your intended use is not permitted by statutory regulation or exceeds the permitted use, you will need to obtain permission directly from the copyright holder. To view a copy of this licence, visit <http://creativecommons.org/licenses/by/4.0/>.

References

1. Hirsch A, Regel J (2022) *Werkzeugmaschinen und vorrichtungen, anforderungen, auslegung, ausfuhrungsbeispiele*. Springer, Berlin <https://doi.org/10.1007/978-3-658-37658-1>
2. Denkena B, Bergmann B, Klemme H (2020) Cooling of motor spindles—a review. *Int J Adv Manuf Technol* 110:3273–3294. <https://doi.org/10.1007/s00170-020-06069-0>

3. Schwenke H, Knapp WH, Haitjema H, Weckenmann A, Schmitt R, Delbressine F (2008) Geometric error measurement and compensation of machines—an update. *CIRP Ann* 57(2):660–675. <https://doi.org/10.1016/j.cirp.2008.09.008>
4. Putz M, Richter C, Regel J, Bräunig M (2018) Industrial relevance and causes of thermal issues in machine tools. In: Ihlenfeldt S (ed) Conference on Thermal Issues in Machine Tools : proceedings : CIRP sponsored conference. Dresden 2018, 1st edn. Verlag Wissenschaftliche Scripten, (<https://nbn-resolving.org/urn:nbn:de:bsz:14-qucosa2-326441>)
5. Tönshoff HK, Denkena B (2004) Spanen, Grundlagen. Springer, Berlin/Heidelberg
6. Vieregge G (1970) Zerspanung der Eisenwerkstoffe. Verlag Stahleisen mbH, Düsseldorf
7. Fischer H (1970) Beitrag zur Untersuchung des thermischen Verhaltens von Bohr- und Fräsmaschinen. Technische Universität Berlin, Dissertation
8. Richardson DJ, Keavey MA, Dailami F (2006) Modelling of cutting induced workpiece temperatures for dry milling. *Int J Mach Tools Manuf* 46:1139–1145
9. Köhler W (2004) Analyse des Einflusses der Schneidenform auf den Hochleistungsbohrprozess. Universität Dortmund. Vulkan Verlag Essen, Dissertation
10. Davies MA, Ueda T, M'Saoubi R, Mullany B, Cooke A (2007) On the measurement of temperature in material removal processes. *CIRP Ann* 56(2):581–604. <https://doi.org/10.1016/j.cirp.2007.10.009>
11. Cui D, Dinghua Z, Baohai W, Ming L (2017) An investigation of temperature and heat partition. *Procedia CIRP* 58:49–54. <https://doi.org/10.1016/j.procir.2017.03.180>
12. Putz M, Schmidt G, Semmler U, Dix M, Bräunig M, Brockmann M, Gierlings S (2015) Heat flux in cutting: importance, simulation and validation. *Procedia CIRP* 31:334–339. <https://doi.org/10.1016/j.procir.2015.04.088>
13. Ustinov A (2018) Experimental investigation and modeling of contact heat transfer. Institute of Heat and Mass Transfer RWTH Aachen <https://doi.org/10.18154/RWTH-2019-10754> (Dissertation)
14. Naumann A, Lang N, Partzsch M, Beitelschmidt M, Benner P, Voigt A, Wensch J (2016) Computation of thermo-elastic deformations on machine tools a study of numerical methods. *Prod Eng* 3:1863–1735. <https://doi.org/10.1007/s11740-016-0674-7>
15. Sauerzapf S, Vettermann J, Naumann A, Saak J, Beitelschmidt M, Benner P (2020) Simulation of the thermal behaviour of machine tools for efficient machine development and online correction of the Tool Center Point (TCP)-displacement (<https://www.euspen.eu/knowledge-base/TI20125.pdf>)
16. Ess M, Weikert S, Wegener K, Mayr J (2012) Dynamic Loads and Thermal Errors on Machine Tools. Report. Institute of Machine Tools and Manufacturing ETH Zurich <https://doi.org/10.3929/ethz-a-007577640>
17. Putz M, Wittstock V, Semmler U, Bräunig M (2016) Simulation-based thermal investigation of the cutting tool in the environment of single-phase fluxes. *Int J Adv Manuf Technol* 83(1–4):117–122. <https://doi.org/10.1007/s00170-015-7488-1>
18. Perri GM, Bräunig M, Gironimo GD, Putz M, Tarallo A, Wittstock V (2016) Numerical modelling and analysis of the influence of an air cooling system on a milling machine in virtual environment. *Int J Ad Manuf Technol* 86(5–8):1853–1864. <https://doi.org/10.1007/s00170-015-8322-5>
19. Putz M, Glänzel J, Regel J, Bräunig M (2019) Effects of cooling lubricant on the thermal regime in the working space of machine tools. *Procedia Manuf* 33:327–334. <https://doi.org/10.1016/j.promfg.2019.04.040>
20. Topinka L, Bräunig M, Putz M, Dix M (2021) Multi-phase simulation of the liquid coolant flow around rotating cutting tool. *MM Sci J* 5:5148–5153. https://doi.org/10.17973/MMSJ.2021_11_2021171
21. Brier S, Regel J, Putz M, Dix M (2021) Unidirectional coupled finite element simulation of thermoelastic TCP-displacement through milling process caused heat load. *MM Sci J* 3:4534–4539. https://doi.org/10.17973/MMSJ.2021_7_2021056
22. Liu H, Helmig T, Augspurger T, Kneer R, Bergs T (2020) A novel FEM-CFD interface for multi-physical simulations to model the effect of cutting fluid on the tool temperature during orthogonal cutting. *SIG. TI. EUSPEN*. (<https://www.euspen.eu/knowledge-base/TI20128.pdf>). Accessed 5 October 2023
23. Tahmasebi E, Albertelli P, Lucchini T, Monno M, Mussi V (2019) CFD and experimental analysis of the coolant flow in cryogenic milling. *Int J Mach Tools Manuf* 140:20–33. <https://doi.org/10.1016/j.ijmachtools.2019.02.003>
24. Peng R, Liu J, Chen M, Tong J, Zhao L (2021) Development of a pressurized internal cooling milling cutter and its machining performance assessment. *Precis Eng* 72:315–329. <https://doi.org/10.1016/j.precisioneng.2021.05.010>
25. Glänzel J, Ihlenfeldt S, Naumann C, Putz M (2017) Decoupling of Fluid and Thermo-elastic Simulations on Machine tools Using Characteristic Diagrams. *Procedia CIRP* 62:340–345. <https://doi.org/10.1016/j.procir.2016.06.068>
26. Naumann C, Riedel I, Ihlenfeldt S, Priber U (2016) Characteristic diagram based correction algorithms for the Thermo-elastic deformation of machine tools. *Procedia CIRP* 41:801–805. <https://doi.org/10.1016/j.procir.2015.12.029>
27. Ihlenfeldt S, Naumann C, Putz M (2018) On the selection and assessment of input variables for the characteristic diagram based correction of thermo-elastic deformations in machine tools. *J Mach Eng* 18:25–38. <https://doi.org/10.5604/01.3001.0012.7630>
28. Naumann C, Glänzel J, Dix M, Ihlenfeldt S, Klimant P (2022) Optimization of characteristic diagram based thermal error compensation via load case dependent model updates. *J Mach Eng* 22(2):43–56. <https://doi.org/10.36897/jme/148181>
29. Jahangeer J, Ramis MK, Jilani G (2007) Conjugate heat transfer analysis of a heat-generating vertical plate. *Int J Heat Mass Transf* 50(1–2):85–93. <https://doi.org/10.1016/j.ijheatmasstransfer.2006.06.042>
30. Topinka L, Prusa R, Huzlik R, Regel J (2023) Definition of a non-contact induction heating of a cutting tool as a substitute for process heat for the verification of a thermal simulation mode. In: Ihlenfeldt S (ed) 3rd International Conference on Thermal Issues in Machine Tools (ICTIMT2023). ICTIMT 2023. Springer, Cham https://doi.org/10.1007/978-3-031-34486-2_24 (Lecture Notes in Production Engineering)
31. Bräunig M, Regel J, Glänzel J, Putz M (2019) Effects of cooling lubricant on the thermal regime in the working space of machine tools. *Procedia Manuf* 33:327–334. <https://doi.org/10.1016/j.promfg.2019.04.040>
32. DAWAEROCIT Schmierungstechnik GmbH (<http://www.dawaerocit.de/>). Accessed 23 March 2020
33. Le Cam L (1986) The central limit theorem around. *Stat Sci* 1:78–96 (<https://www.jstor.org/stable/2245503>)
34. Dekking FM, Kraaikamp C, Lopuhaä HP, Meester LE (2005) A modern introduction to probability and statistics. Springer, London <https://doi.org/10.1007/1-84628-168-7>
35. König K (2008) Fertigungsverfahren 1 – Drehen, Fräsen, Bohren, 8th edn. Springer, p 265f <https://doi.org/10.1007/978-3-540-35834-3>
36. Pabst R (2008) Mathematische Modellierung der Wärmestromdichte zur simulation des thermischen Bauteilverhaltens bei der Trockenebearbeitung. Universität Karlsruhe (TH) <https://doi.org/10.5445/IR/1000009954> (Dissertation)
37. Matsuda K, Tanaka R, Sekiya K, Yamada K (2019) Cutting force changes during one cut in end milling with a throw-away insert

- difference between up-cut and down-cut. KEM 825:123–128 (<https://www.scientific.net/KEM.825.123>)
38. Ansys CFX-Solver Theory Guide Release 2021 R2
39. Ballesteros Martínez M, Pereyra E (2020) CFD study and experimental validation of low liquid-loading flow assurance in oil and gas transport: studying the effect of fluid properties and operating conditions on flow variables. *Heliyon*. <https://doi.org/10.1016/j.heliyon.2020.e05705>
40. Brackbill JU, Kothe DB, Zemach C (1992) A continuum method for modeling surface tension. *J Comput Phys* 100(2):335–354. [https://doi.org/10.1016/0021-9991\(92\)90240-Y](https://doi.org/10.1016/0021-9991(92)90240-Y)
41. Matweb material property database. <http://www.Matweb.com>. Accessed 15 May 2023
42. ANSYS CFX Material Database
43. Spur G, de Haas P (1974) Thermal Behaviour of NC Machine Tools. In: Koenigsberger F, Tobias SA (eds) Proceedings of the Fourteenth International Machine Tool Design and Research Conference. Palgrave, London https://doi.org/10.1007/978-1-349-01921-2_36
44. Wan J (2021) The heat transfer coefficient predictions in engineering applications. *J Phys Conf Ser*. <https://doi.org/10.1088/1742-6596/2108/1/012022>
45. Höhne T, Porombka P, Moya S (2020) Validation of AIAD sub-models for advanced numerical modelling of horizontal two-phase flows. *Fluids*. <https://doi.org/10.3390/fluids5030102>
46. ANSYS Meshing User's Guide Release 2021 R2
47. Gonzales O, Andrew M (2008) A first course in continuum mechanics. Cambridge University Press, Cambridge <https://doi.org/10.1017/CBO9780511619571>
48. Härdle WK, Simar L (2015) Applied multivariate statistical analysis. Springer, Berlin <https://doi.org/10.1007/978-3-662-45171-7>
49. Spiess AN, Neumeyer N (2010) An evaluation of R2 as an inadequate measure for nonlinear models in pharmacological and biochemical research: a Monte Carlo approach. *BMC Pharmacol* 10:6. <https://doi.org/10.1186/1471-2210-10-6>
50. Sobol IM (1967) On the distribution of points in a cube and the approximate evaluation of integrals. *USSR Comput Math Math Phys*. [https://doi.org/10.1016/0041-5553\(67\)90144-9](https://doi.org/10.1016/0041-5553(67)90144-9)

Publisher's Note Springer Nature remains neutral with regard to jurisdictional claims in published maps and institutional affiliations.